JMEPEG (2006) 15:558-563
DOI: 10.1361/105994906X136124

1059-9495/$19.00

High-Temperature Corrosion of Y-Doped Fe_3Al in Environments Containing Chlorine and Oxygen

W.D. Cho and Gilsoo Han

(Submitted November 2, 2005; in revised form November 29, 2005)

The high-temperature corrosion performance of Y-doped Fe_3Al was studied in various environments containing chlorine, oxygen, and argon. Results were compared with Y-free Fe_3Al in terms of corrosion rate and microstructure of corrosion products. The kinetic pattern shown in the two types of alloy features two consecutive stages: initial slow mass loss followed by fast linear mass loss. However, addition of Y decreased the rate but increased the duration of the first stage of the corrosion. Microstructure examination indicates that the beneficial effect of Y may be due to the formation of pegs and the development of dense oxide layers.

Keywords corrosion, iron aluminide, reactive element, Y

1. Introduction

Thermogravimetric measurements for the corrosion of pure Fe_3Al and Y-doped Fe_3Al were conducted under three different conditions: at 700 °C in Ar-2% Cl_2; at 700 °C in Ar-0.5% Cl_2-0.1% O_2; and at 800 °C in Ar-1% Cl_2. It is well known that the presence of chlorine in oxidizing environments causes not only an increase in corrosion rate but also a change in corrosion mode and mechanism. In an earlier study (Ref 1) on corrosion of Fe_3Al in 1% Cl_2/Ar atmosphere in the temperature range 750-900 °C, corrosion occurred in two distinct consecutive stages: slow linear mass loss and subsequent fast linear mass loss. The initial slow weight loss is due to formation of Al_2O_3, which suppresses evaporation of metal chlorides. The second stage of corrosion, characterized as the fast linear mass loss, is controlled by the mass transfer of gaseous $FeCl_2$ in the gas phase. In this study, continuous investigations have been carried out to study the effect of Y, a reactive element, on the corrosion of Fe_3Al doped with Y in environments containing various mixtures of oxygen and chlorine.

Reactive elements, such as Y, Zr, and other rare earths, have been known to improve the oxidation resistance of high-temperature alloys. The effects of reactive elements on the oxidation behavior of alumina-forming alloys are as follows (Ref 2, 3): (a) improvement of alumina-scale adhesion; (b) change in aluminum oxide growth mechanism; and (c) decrease of aluminum oxide grain size. Improvement in alumina-scale adhesion is important in corrosive environments because, as mentioned in the previous paragraph, spallation of the oxide during oxidation or cooling decreases the oxidation resistance. The mechanisms for improvement in adhesion can be classified into the following major groups: (a) pegging mechanism, (b) sulfur-effect mechanism, (c) vacancy sink mechanism, and (d) improvement of bond strength at the interface.

W.D. Cho and **Gilsoo Han,** Department of Metallurgical Engineering, University of Utah, Salt Lake City, UT 84112. Contact e-mail: wdcho@mines.utah.edu.

The pegging mechanism is one of the most widely known mechanisms for the adhesion improvement of oxide scale. The effects of Y and/or Hf on the oxidation of alloys were extensively studied by many researchers (Ref 4-7). These authors found that the oxide scale on the alloys containing small amounts of reactive elements developed numerous pegs that formed around the oxide particles of the reactive elements in the alloy substrate. These pegs penetrated into the alloy and appeared to be concentrated at the grain boundaries of the alloy substrate. Thus, it was suggested that these pegs mechanically anchored the oxide scale to the alloy substrate, which led to improvement in adhesion of the oxide scale.

Many studies (Ref 8-11) revealed that segregation of sulfur at the oxide/alloy interface weakened the bonding strength between the protective oxide and the substrate alloy and that the addition of a reactive element, such as Y or Ce, reduced sulfur segregation at the oxide/alloy because the reactive elements are strong sulfide formers. Thus, adhesion of oxides can be improved by adding a reactive element to the alloy, which forms a more adherent oxide. Voids formed at the oxide/alloy interface by the oxidation process act as local stress-concentration sites during cooling, which thus initiate cracking or spallation of the oxide scale. Several investigators (Ref 7, 12-14) studied the effects of reactive elements on void formation at the oxide/alloy interface, which led to the proposal of a vacancy sink mechanism. Addition of reactive elements, such as Y and Hf, was found to reduce the porosity at the oxide/alloy interface, which in turn may have resulted from the modification of the oxide growth mechanism. Addition of a reactive element enhanced the inward transport of oxygen and hindered the outward diffusion of the metal cation (Ref 13, 14). Due to reduced porosity at the interface, adhesion of the oxide scale may be improved.

As discussed above, the small addition of reactive elements to the various alloys is beneficial to improving corrosion resistance in oxidizing environments. However, no investigation has been done into the effect of reactive elements on the corrosion in oxygen/chlorine-containing environments. In this study, corrosion of Fe_3Al containing 0.4 wt.% Y in mixed environment has been investigated and compared with the alloy

without Y in terms of kinetics, microstructure, and corrosion mechanism.

2. Materials and Experimental Procedures

The alloys used in this study were made of 99.98% iron lumps, 99.9% aluminum granules, and 99.9% Y powder (40 mesh) in a vacuum arc furnace. All ingots were subsequently homogenized at 1000 °C in an Ar atmosphere for 12 h. The ingots were then cut into elliptical shapes for corrosion specimens using a diamond saw. The specimens were then abraded and polished using a diamond suspension (up to 1 μm). After polishing, each specimen was degreased and cleaned in an ultrasonic cleaner containing acetone and rinsed with methanol. The specimen was analyzed using inductively coupled plasma (ICP) and a LECO carbon and sulfur analyzer, and x-ray diffraction (XRD) was performed to confirm the composition and phase of the specimens. The composition of the iron aluminides was Fe-24.1 at.% Al-0.002 wt.% S and Fe-22.0 at.% Al-0.40 wt.% Y-0.002 wt.% S. The experimental apparatus used for these experiments has been described elsewhere in detail (Ref 1) and consists of a computer-controlled microbalance, a kanthal-wound furnace, a gas train for purification, and mixing chambers for the reagent gases. Before the ultrahigh-purity Ar was supplied to the furnace or to the mixing chamber, the gas was dried and purified by passage through columns of Drierite and Cu turnings to remove H_2O and O_2, respectively. The gas tubing was a fluoropolymer tube to prevent penetration of moisture and other gases from the air to the system.

The alloy specimen was loaded with Pt-wire (0.05 mm diameter) inside a fused quartz reaction tube. The reaction tube was flushed with argon at a flow rate of 100 mL/min for 2 h to remove residual oxygen in the tube. The purified argon gas flow was maintained until the desired temperature was obtained. A very thin layer of aluminum oxide was observed to form on the surface of the specimen during heating (~2 h) from room temperature to the reaction temperature. After the temperature of the furnace reached the reaction temperature and was stable under the Ar atmosphere, a 1% Cl_2-Ar gas mixture containing ~1 ppm of oxygen was introduced into the reaction tube at a flow rate of 100 mL/min, with a superficial flow rate of ~1 cm/s. The Reynolds number calculation in this flowing condition showed a laminar gas flow. From this point, the mass change of the specimen was measured using a balance with 1 μg sensitivity. After the predetermined reaction time, the specimens were cooled in the furnace under the Ar and removed for microstructure examination. Corrosion products were characterized by XRD, scanning electron microscopy (SEM), and energy-dispersive spectrometry (EDS).

3. Results and Discussion

3.1 Thermogravimetric Results

Figure 1 shows thermogravimetric results of the corrosion of both pure and Y-doped Fe_3Al in three different corrosion conditions: Ar-2% Cl_2 gas mixture at 700 °C; Ar-1% Cl_2 gas mixture at 800 °C; and Ar-0.5% Cl_2-0.1% O_2 gas mixture at 700 °C. Although the second-stage of corrosion did occur in experiments for both specimens in the Ar-2% Cl_2 gas mixture

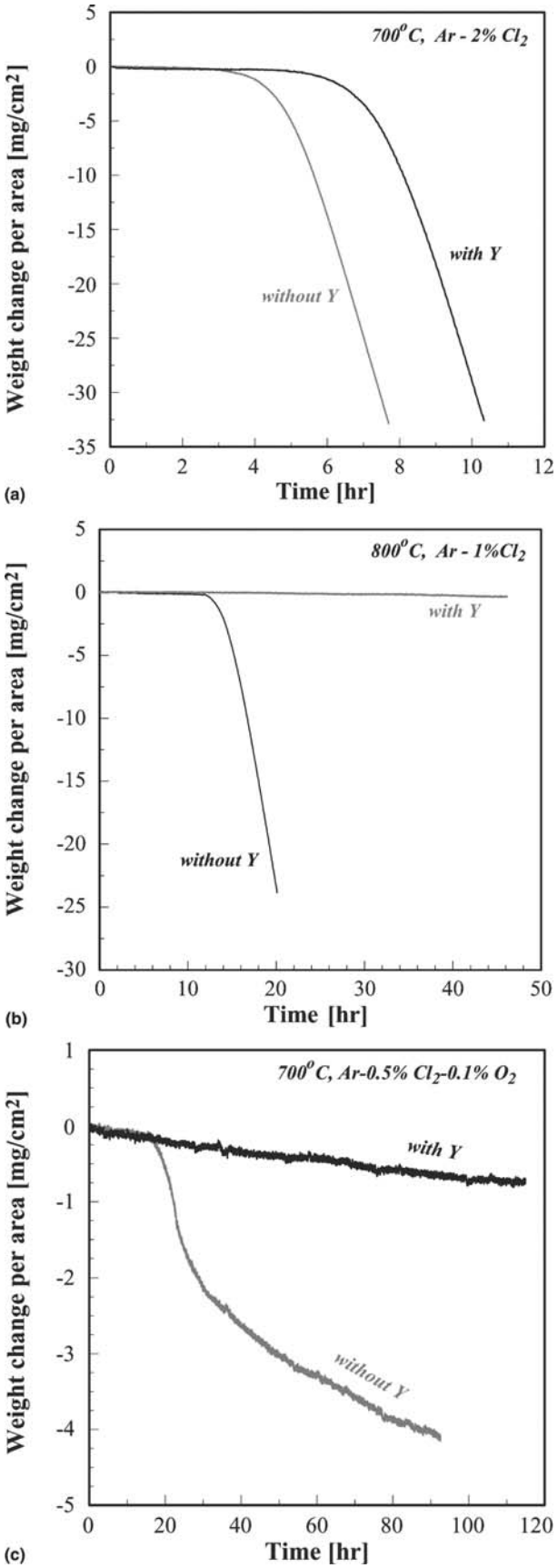

Fig. 1 Thermogravimetric results of the corrosion of Y-doped and undoped Fe_3Al: (a) in Ar-2% Cl_2 gas mixture at 700 °C; (b) in Ar-1% Cl_2 gas mixture at 800 °C; (c) in Ar-0.5% Cl_2-0.1% O_2 gas mixture at 700 °C

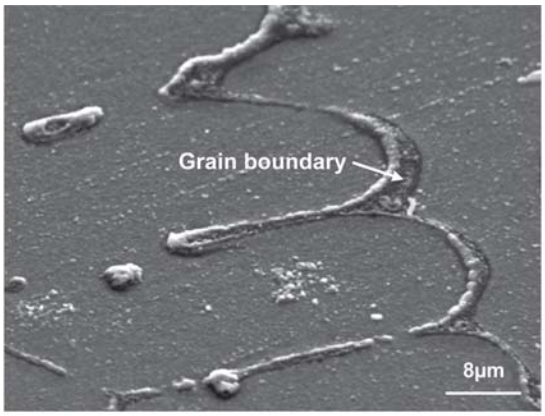

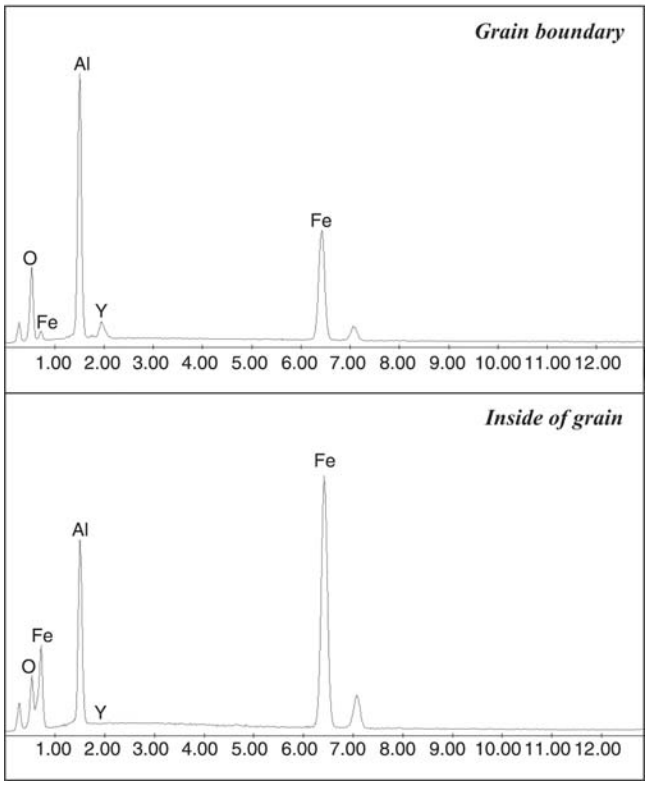

Fig. 2 SEM micrograph and EDS analysis for the grain boundary and bulk of the grain on the surface of Y-doped specimen after heating to 700 °C in Ar atmosphere and cooling to room temperature

at 700 °C, it was not observed for the Y-doped Fe_3Al in the Ar-0.5% Cl_2-0.1% O_2 gas mixture at 700 °C for 100 h and in the Ar-1% Cl_2 gas mixture at 800 °C for 40 h. Despite the differences in the corrosion behavior, some beneficial effects of Y-doping on the corrosion of Fe_3Al can be seen from the thermogravimetric results. One beneficial effect is that the corrosion rate of the first stage decreases by adding Y from 55.1 to 32.6 $\mu g/cm^2 \cdot h$ in Ar-2% Cl_2 at 700 °C; from 16.8 to 7.9 $\mu g/cm^2 \cdot h$ in Ar-1% Cl_2 at 800 °C; and from 7.3 to 6.2 $\mu g/cm^2 \cdot h$ in Ar-0.5% Cl_2-0.1% O_2 at 700 °C. However, the corrosion rate of the second stage in Ar-2% Cl_2 is not affected by the presence of Y. The other beneficial effect of Y is the increase in the duration of the first stage of the corrosion. These results suggest that Y may retard the formation or evaporation of gaseous aluminum chloride during the first stage by improving the properties of the oxide formed on the alloy, which can be illustrated through microstructure investigation of the corrosion products.

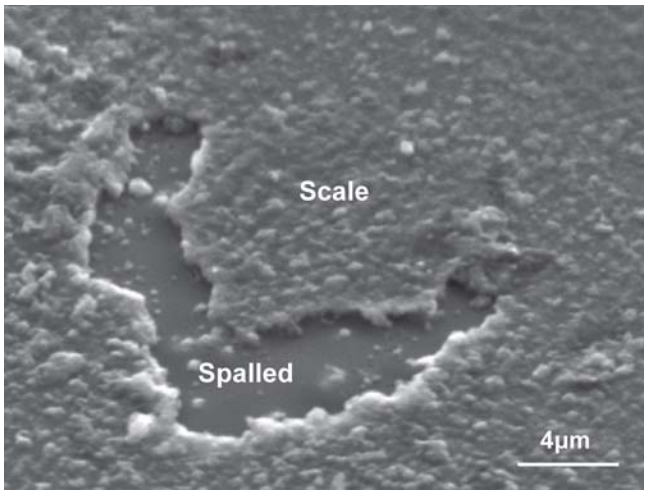

Fig. 3 SEM micrograph for the surface of a specimen without Y after heating to 700 °C in Ar atmosphere and cooling to room temperature

3.2 Microstructure of Corrosion Products

The surface morphologies of Y-doped and undoped specimens after raising the temperature to 700 °C in pure Ar and cooling down to room temperature were examined by SEM and EDS (Fig. 2 and 3). This surface condition is important because it is the initial condition before the high-temperature corrosion test. As seen in the figures, the morphologies are considerably different between Y-doped and undoped specimens. The surface of the specimen containing Y is covered with metal oxides, and swollen lines are observed along the grain boundaries. The EDS data (Fig. 2) of the surface oxide show segregation of Y along the grain boundaries. It is not clear what type of metal oxide is on the surface because the oxide is too thin to measure its composition and structure by EDS and XRD. As reported in several other investigations (Ref 15-18), however, it may be aluminum and Y oxide. On the other hand, the surface of the undoped specimen is flat, and some part of surface oxide spalled off while the specimen cooled to room temperature. This spallation was not observed in the specimen containing Y, indicating that the Y-doped iron aluminide has a more adhesive oxide layer to the matrix than did Y-free Fe_3Al. This improvement of oxide adhesion may be one of the reasons for the beneficial effect of Y on the corrosion resistance.

The surface morphology of the Y-doped specimen varied with exposure time during the first stage of the corrosion. Reactions readily occurred at the area containing Y, such as at grain boundaries as shown in Fig. 4, indicating that the presence of Y at the grain boundaries promotes reactions in the corrosion environment. These corrosion reactions produce many flake-type corrosion products composed mainly of Al, O, and Y. Thus, the products may be aluminum and Y oxides, such as Al_2O_3, Y_2O_3, or $Y_3Al_5O_{12}$. These oxides, which preferentially formed along the grain boundaries, could restrain chlorine from diffusing into metal-oxide interface and forming metal chlorides. As shown in Fig. 4, no spallation of oxide layer was detected for short-term exposure to the corrosion environments, which may be due to the improvement in adhesion of the initial-state oxide caused by the presence of Y.

The pegging mechanism was described earlier to support the favorable effects of Y addition. As shown in Fig. 5, the pegs were observed at the grain boundaries during the first

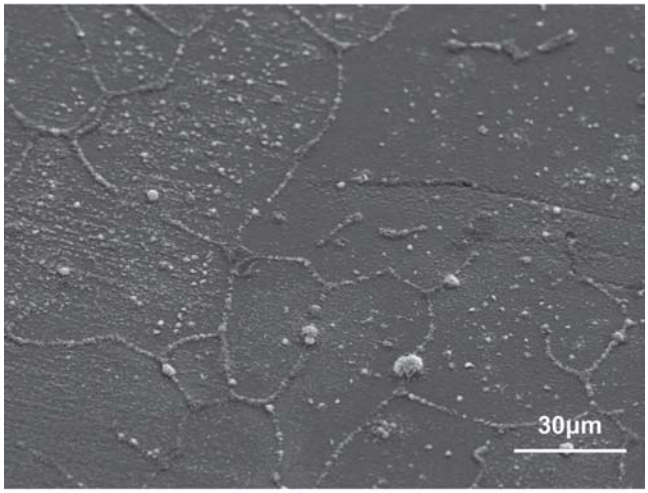

(a)

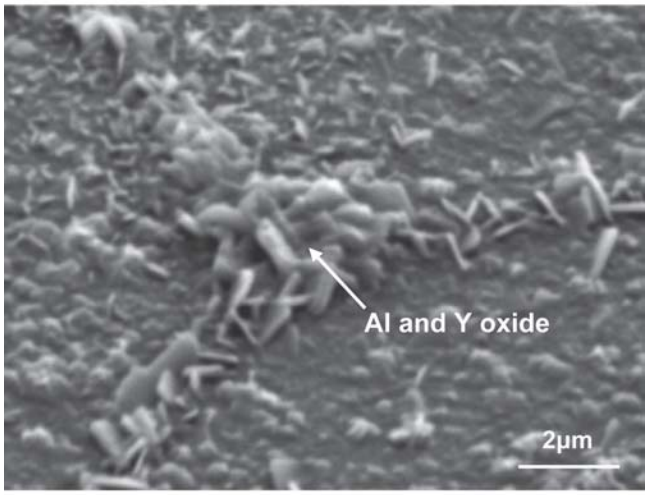

(b)

Fig. 4 SEM micrographs for the Y-doped specimen after corrosion test at 700 °C: (a, b) in Ar-2% Cl_2 for 2 h

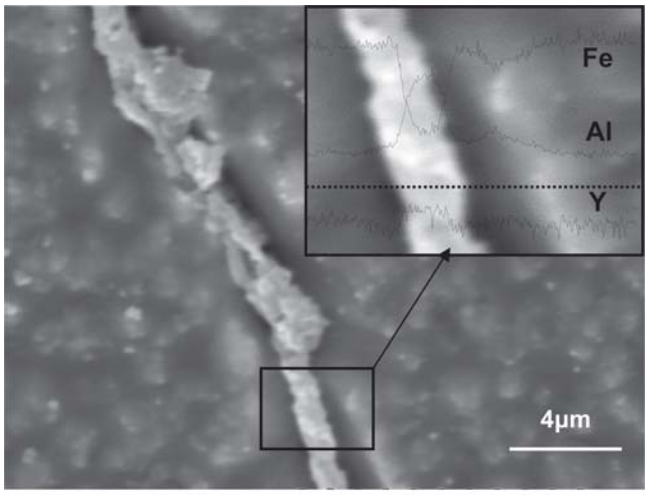

(a)

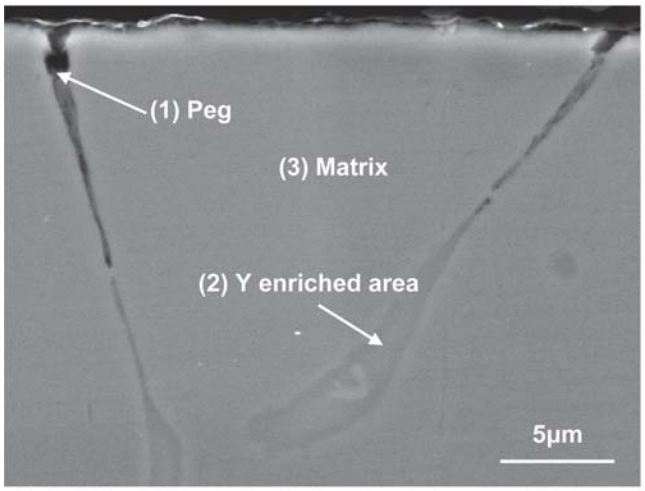

(b)

Fig. 5 SEM micrographs and composition profile for the Y-doped specimen in the first stage of the corrosion: (a) grain boundary area after removing outer corrosion products; (b) cross-section area showing grain boundaries

stage of corrosion, which is related to preferred oxidation due to segregation of Y along the grain boundaries. The pegs are mainly aluminum and Y oxide, as illustrated by EDS analysis in Fig. 6. These pegs can mechanically anchor the oxide layer to the matrix, resulting in adhesion improvement of the oxide layer. During the first stage, the Y-doped Fe_3Al forms Al and Y oxides along the grain boundaries, which makes inward diffusion of chlorine slow, and also develops an adhesive and dense aluminum oxide layer that is more protective against chlorine attack.

As shown in Fig. 1(a), both undoped and Y-doped specimens are subject to fast, continuous linear mass loss during the second stage of corrosion, and the corrosion rates are about the same. Well-developed pegs were also observed during the second stage, as shown in Fig. 7. The corrosion takes place along the grain boundaries of the specimen, and the corrosion product consists of metal oxides and metal chlorides confirmed by EDS analysis, as shown in Fig. 8. In an earlier investigation on corrosion of Fe_3Al in Cl_2/O_2 environments (Ref 1), the mechanism of the second corrosion stage is characterized by iron chlorination and aluminum active oxidation. Although addition of Y may slow down the first corrosion stage, the same mechanism can be applied to the second corrosion stage for the Y-doped specimens. Once the chlorine penetrates the oxide and grain boundaries, it reacts with iron and aluminum.

During the first corrosion stage, aluminum continuously diffuses out from the bulk alloy specimen to the oxide/metal interface and reacts with chlorine to form a volatile compound, causing depletion of aluminum at some localized areas. As the depth of the aluminum-depletion zone increases, the activity of aluminum on the metal/scale interface decreases, and thus the tendency of iron to react with chlorine increases. Therefore, a subsequent rapid reaction between chlorine and iron takes place, followed by the evaporation of $FeCl_2$ due to its high vapor pressure. A small part of the gaseous iron chloride is converted into iron oxide because the equilibrium oxygen partial pressure for the active oxidation of iron chloride is relatively high. Evaporating iron chloride that is not converted into oxide diffuses into the gas phase, which leads to the fast mass loss of the specimen. However, due to the high vapor pressure of aluminum chloride and the very low equilibrium oxygen partial pressure of the active oxidation of aluminum chloride,

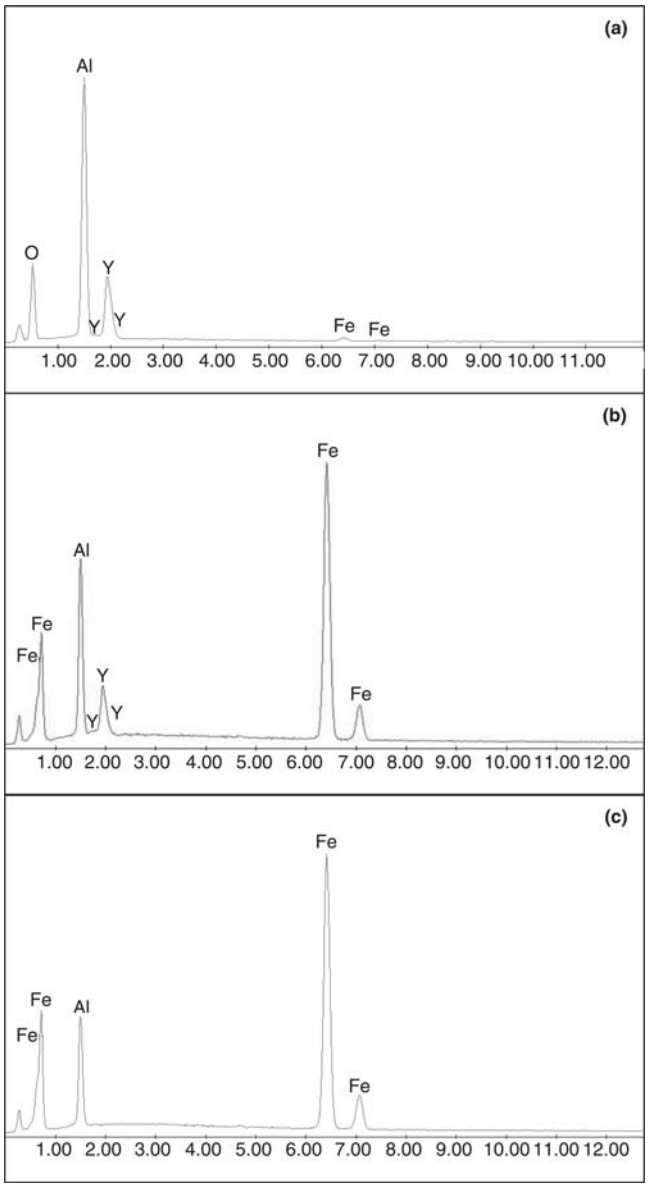

Fig. 6 EDS data for the Y-doped specimen in the first stage of the corrosion: (a) peg, area (1) in Fig. 5(b); (b) Y-enriched area, area (2) in Fig. 5(b); (c) alloy matrix, area (3) in Fig. 5(b)

much more aluminum oxide is formed than iron oxide. In other words, active oxidation for aluminum chloride can occur at a much lower oxygen partial pressure than that for iron chloride because the equilibrium constant for the active oxidation of aluminum chloride is much higher than that of iron chloride. The oxide produced in this stage is no longer dense and protective due to the high vapor pressure of the iron chloride gas that coexists with aluminum chloride. Accordingly, the rate of mass loss in the second stage is very fast due to the formation of volatile iron chloride.

4. Conclusions

Corrosion of undoped Fe_3Al in the gas mixtures containing chlorine at 700 and 800 °C consists of two consecutive stages: (1) slow linear mass loss stage and (2) subsequent fast linear

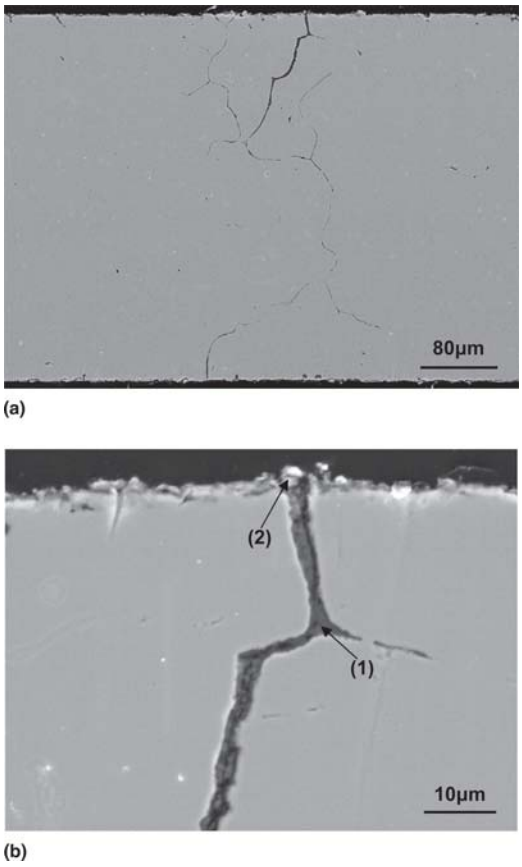

Fig. 7 SEM micrographs for the Y-doped specimen in the second stage of the corrosion in Ar-2%Cl_2 at 700 °C: (a) lower magnification; (b) higher magnification: (1) surface corrosion product and (2) inner corrosion product

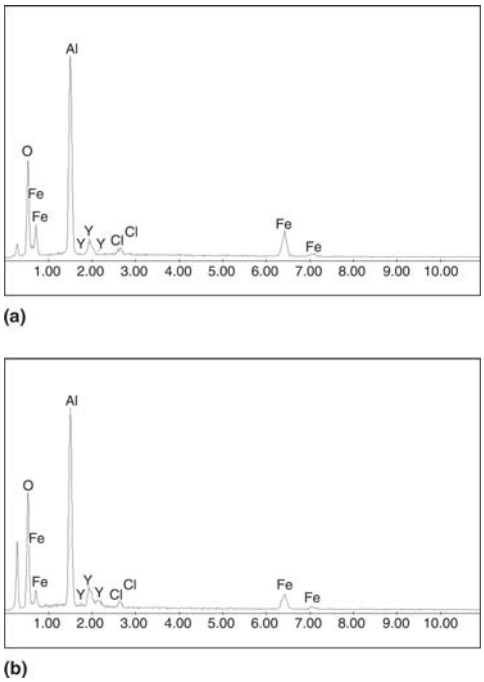

Fig. 8 EDS data for localized corrosion product of the Y-doped specimen in the second stage of the corrosion in Ar-2%Cl_2 at 700 °C: (a) inner corrosion product, area (1) in Fig. 7(b); (b) outer corrosion product, area (2) in Fig. 7(b)

mass loss stage. The Y-doped Fe_3Al exhibited a similar kinetic pattern but much better corrosion resistance under the same corrosion conditions. Addition of Y decreases the rate but increases the duration of the first corrosion stage. The Y-doped Fe_3Al forms an aluminum oxide layer with strong adhesion to the matrix or with fewer defects to make the alloy more protective against chlorine attack. Microstructure analysis after corrosion indicates formation of pegs along the grain boundaries. The pegs may anchor the oxide layer to the alloy matrix, which may improve corrosion resistance.

Acknowledgment

Financial support from the National Science Foundation under grant CMS-9818395 is gratefully acknowledged.

References

1. G. Han and W.D. Cho, High-Temperature Corrosion of Fe_3Al in 1% Cl_2/Ar Atmosphere, *Oxid. Met.,* 2002, **58**(3/4), p 391-413
2. A.M. Huntz, Effect of Active Elements on the Oxidation Behavior of Al_2O_3-Formers, *The Role of Active Elements in the Oxidation Behavior of High Temperature Metals and Alloys,* E. Lang, Ed., Elsevier Applied Science, London, 1989, p 81-109
3. F.H. Stott and G.C. Wood, Growth and Adhesion of Oxide Scales on Al_2O_3-Forming Alloys and Coatings, *Mater. Sci. Eng.,* 1987, **87,** p 267-274
4. I.M. Allam, D.P. Whittle, and J. Stringer, Oxidation Behavior of Co-CrAl Systems Containing (Hf + Yt) Active Element Additions, *Oxid. Met.,* 1978, **12,** p 35-66
5. E.J. Felton, High-Temperature Oxidation of Fe-Cr Base Alloys with Particular Reference to Fe-Cr-Y, *J. Electrochem. Soc.,* 1961, **108,** p 490-495
6. H. Hindam and D.P. Whittle, Peg Formation by Short-Circuit Diffusion in Al_2O_3 Scales Containing Oxide Dispersions, *J. Electrochem. Soc.,* 1982, **129,** p 1147-1149
7. C.S. Giggins and F.S. Pettit, Oxidation of TD NiC(Ni-20Cr-2 vol pct ThO_2) between 900 and 1200 °C, *Met. Trans.,* 1971, **2,** p 1071-1078
8. J.G. Smeggil, A.W. Funkenbusch, and N.S. Bornstein, A Relationship between Indigenous Impurity Elements and Protective Oxide Scale Adherence Characteristics, *Metall. Trans. A,* 1986, **17A,** p 923-932
9. A.W. Funkenbusch, J.G. Smeggil, and N.S. Bornstein, Reactive Element-Sulfur Interaction and Oxide Scale Adherence, *Metall. Trans. A,* 1985, **16A,** p 1164-1166
10. K. Kasahara, Y. Ikeda, T. Kimura, and T. Tsujimoto, Effects of Additions of Y and Rare-Earth Metals on the Cyclic Oxidation of TiAl Alloys, *J. Jpn. Inst. Met.,* 1996, **60,** p 907-913
11. T.G. Rhys-Jones, Use of Cerium and Cerium Oxide Additions to Improve High Temperature Oxidation Behaviour of Fe-Cr Alloys, *Mater. Sci. Technol.,* 1988, **4,** p 446-454
12. J.K. Tien and F.S. Pettit, Mechanism of Oxide Adherence on Fe-25Cr-4Al (Y or Sc) Alloy, *Metall. Trans.,* 1972, **3,** p 1587-1599
13. W.J. Quadakkers, H. Holzbrecher, K.G. Briefs, and H. Beske, Differences in Growth Mechanisms of Oxide Scales Formed on ODS and Conventional Wrought Alloys, *Oxid. Met.,* 1989, **32,** p 67-88
14. E.W.A. Young and J.H.W. de Wit, An ^{18}O Tracer Study on the Growth Mechanism of Alumina Scales on NiAl and NiAlY Alloys, *Oxid. Met.,* 1986, **26,** p 351-361
15. P.F. Tortorelli and K. Natesan, Critical Factors Affecting the High-Temperature Corrosion Performance of Iron Aluminides, *Mater. Sci. Eng.,* 1998, **A258,** p 115-125
16. A. Velon and I. Olefjord, Oxdation Behavior of Ni_3Al and Fe_3Al: II. Early Stage of Oxide Growth, *Oxid. Met.,* 2001, **56,** p 425-452
17. P. Tomaszewicz and G.R. Wallwork, Observation of Nodule Growth During the Oxidation of Pure Binary Iron-Aluminum Alloys, *Oxid. Met.,* 1983, **19,** p 165-185
18. J.H. DeVan and P.F. Tortorelli, The Oxidation-Sulfidation Behavior of Iron Alloys Containing 16-40 at% Aluminum, *Corros. Sci.,* 1993, **35,** p 1065-1071